Journal of Materials Chemistry A

ROYAL SOCIETY OF CHEMISTRY

PAPER

View Article Online
View Journal | View Issue

Cite this: J. Mater. Chem. A, 2022, 10, 20018

A hexacoordinated Bi^{3+}-based ellagate MOF with acid/base resistance boosting carbon dioxide electroreduction to formate†

Junjun Li,‡[a] Congyong Wang,‡[bd] Dingjia Wang,‡[c] Chenhuai Yang,‡[a] Xiaoya Cui,[ef] Xuejiao J. Gao *[c] and Zhicheng Zhang *[a]

Received 4th March 2022
Accepted 14th July 2022

DOI: 10.1039/d2ta01727j

rsc.li/materials-a

Electrochemical conversion of CO_2 into energy-dense liquids, such as formic acid, as hydrogen carriers and chemical feedstocks is desirable. However, the development of highly efficient and stable electrocatalysts toward formate production in a wide potential window still remains a great challenge. Herein, rod-shaped bismuth ellagate metal–organic framework (referred to as SU-101) catalysts were demonstrated to exhibit excellent activity, selectivity, and stability for the conversion of CO_2 into $HCOO^-$. In particular, the SU-101 nanorods (NRs) achieved a high $HCOO^-$ Faraday efficiency (FE) up to 93.66% at −1.10 V *vs.* RHE and a partial current density of −14.57 mA cm^{-2}. Significantly, the FE of $HCOO^-$ could be maintained over 87.51% during 10 hours of continuous electrolysis without significant deterioration. The results indicated that the excellent performance could be attributed to the special structure of $Bi_2O(H_2O)_2(C_{14}H_2O_8)\cdot nH_2O$ (SU-101). DFT calculations show that the unique hexacoordinated Bi^{3+} site of SU-101 is highly efficient for formate production with very low overpotentials. This work paves a way to develop a Bi-MOF as a highly stable, molecularly tunable catalytic material for selective CO_2 reduction to specific valuable chemicals.

Zhicheng Zhang is a Professor at the Department of Chemistry, School of Science, Tianjin University. He received his PhD degree from the College of Chemical Engineering, China University of Petroleum (Beijing) in 2012. Then, he worked as a Postdoctoral Researcher at the Department of Chemistry, Tsinghua University. In 2014, he began working as a Research Fellow at the School of Materials Science and Engineering, Nanyang Technological University, Singapore. In 2019, he joined Tianjin University as a Full Professor. His research interests include the design and synthesis of functional nanomaterials and their applications in energy conversion and catalysis.

Introduction

The electrochemical CO_2 reduction reaction (CO_2RR) has been considered one of the most attractive pathways to convert CO_2 into useful feedstocks and fuels, which can mitigate environmental issues and alleviate the energy crisis.[1–6] Formic acid or formate, as a common liquid CO_2 reduction product, has been widely applied in livestock feed as a preserving and antibacterial agent, as liquid fuel in direct formate fuel cells, and in textile and leather production.[7–9] Significant efforts have been devoted to exploring and designing novel electrocatalysts for producing value-added products, such as formate.[1,5,10,11]

In recent years, various metal-based electrocatalysts, such as Bi, In, Sn, Pb, Pd, Cu, Hg, *etc.*,[12–21] have been proven to be active in reducing CO_2 into formate. Notably, Bi-based catalysts have been considered suitable candidates owing to their captivating characteristics: (i) compared to the toxic metals of Pb and Hg, Bi-based electrocatalysts display lower toxicity and an

[a]Tianjin Key Laboratory of Molecular Optoelectronic Sciences, Department of Chemistry, School of Science, Tianjin University, Collaborative Innovation Center of Chemical Science and Engineering, Tianjin 300072, China. E-mail: zczhang19@tju.edu.cn

[b]Joint School of National University of Singapore and Tianjin University, International Campus of Tianjin University, Binhai New City, Fuzhou 350207, China

[c]College of Chemistry and Chemical Engineering, Jiangxi Normal University, Nanchang 330022, China. E-mail: gaoxj@jxnu.edu.cn

[d]Department of Chemistry, Faculty of Science, National University of Singapore, Singapore 117543, Singapore

[e]Ministry of Education Key Laboratory of Protein Sciences, Beijing Advanced Innovation Center for Structural Biology, School of Life Sciences, Tsinghua University, Beijing 100084, China

[f]Beijing Frontier Research Center for Biological Structures, Tsinghua University, Beijing 100084, China

† Electronic supplementary information (ESI) available. See https://doi.org/10.1039/d2ta01727j

‡ These authors contributed equally to this work.

environmentally benign nature; (ii) their high hydrogen evolution overpotential is beneficial for promoting CO_2 reduction; (iii) Bi-based electrocatalysts exhibit strong affinity toward OCHO intermediates, giving rise to high selectivity for formate production; (iv) their low cost and good durability can facilitate their practical application. Recently, Bi-based metal–organic frameworks (MOFs) have attracted considerable interest for electrocatalysis due to their readily accessible active sites, tailored porosity, convenient functionalization, and large specific surface area.[22–27] To date, there have been very few reports on the application of MOFs in the CO_2RR, thus deserving an in-depth exploration and understanding of Bi-based MOF electrocatalysts.[28,29] However, the reported Bi-based MOFs usually suffer from structural degradation and rearrangement at reducing potentials during the CO_2RR process,[6,12,30] which would lead to the complexity of the study of the catalytic mechanism. Therefore, the rational design and synthesis of Bi-based MOFs with robust structural stability is of great significance to the development of highly efficient electrocatalysts for the conversion of CO_2 into $HCOO^-$.

To effectively tackle this issue, we fabricated highly stable $Bi_2O(H_2O)_2(C_{14}H_2O_8)\cdot nH_2O\cdot nH_2O$ (SU-101) nanorod (NR) catalysts *via* a facile wet chemical method at room temperature. Impressively, the crystalline structure of the SU-101 NRs could be well maintained over a large pH range (from 2 to 14). The as-prepared SU-101 NRs exhibited high activity and selectivity toward $HCOO^-$ for electrochemical CO_2 reduction under ambient conditions, with an excellent faradaic efficiency (FE) up to 93.66% and a partial current density as high as 14.57 mA cm^{-2} at −1.06 V *versus* the reversible hydrogen electrode (*vs.* RHE). Moreover, it was also found that the SU-101 NRs are capable of retaining their good structure and chemical stability after a long-term electrocatalytic process. DFT calculation results indicated that the outstanding performance could be attributed to the unique hexacoordinated Bi^{3+} site of SU-101. The adsorption of CO_2 on the central Bi site is mainly

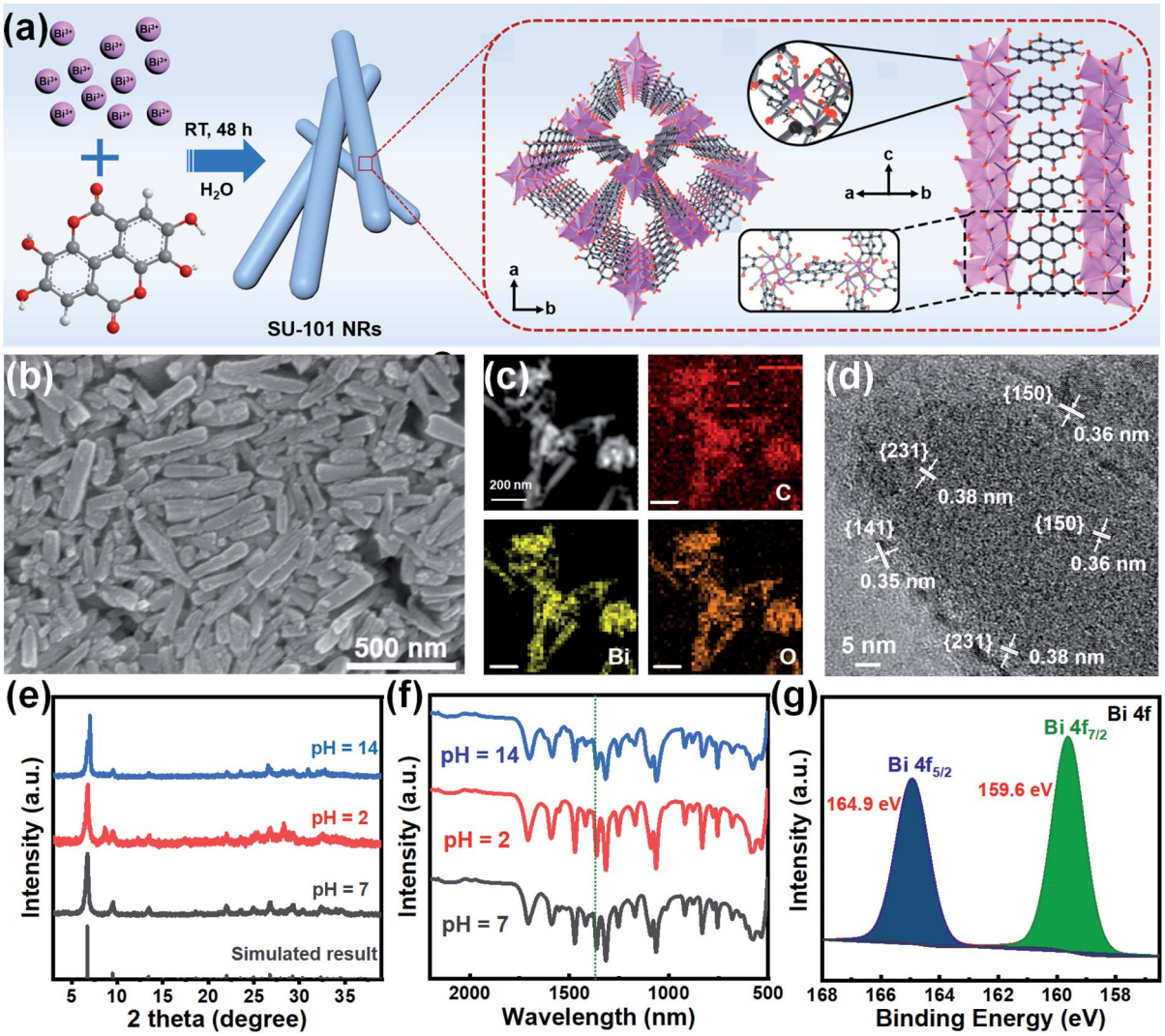

Fig. 1 (a) Schematic illustration of the preparation procedure of the SU-101 NRs. (b) SEM image of the SU-101 NRs. (c) HAADF-STEM and the corresponding EDS elemental mapping images of Bi, O, and C. (d) HRTEM image of the SU-101 NRs. (e) PXRD patterns and (f) FT-IR spectra of the SU-101 NRs treated with different pH solutions. (g) Bi XPS spectrum of the SU-101 NRs.

achieved by coordination interaction. The active Bi sites exhibit moderate adsorption strength, which is neither so weak as to allow the hydrogen evolution reaction (HER) to occur preferentially nor so strong as to cause CO formation, resulting in high selectivity toward $HCOO^-$ production.

Results and discussion

The SU-101 NRs were synthesized in the presence of ellagic acid, bismuth acetate, and glacial acetic acid *via* a facile wet chemical method, as schematically illustrated in Fig. 1a and S1.† Scanning electron microscope (SEM) and transmission electron microscopy (TEM) images show the rod-like morphology with an average length and width of 334.9 nm and 69.2 nm, respectively (Fig. 1b, S2 and S3†). High angle annular dark-field scanning TEM (HAADF-STEM) and corresponding energy dispersive spectroscopy (EDS) element mapping images of the as-synthesized SU-101 NRs confirm the homogeneous distribution of Bi, C, and O elements (Fig. 1c). The HRTEM image of the SU-101 NRs shows obvious lattice fringes with lattice spacings of 0.35 nm, 0.36 nm and 0.38 nm, which can be assigned to the {141}, {150}, and {231} crystal planes of SU-101 (Fig. 1d). Their powder X-ray diffraction (PXRD) patterns (Fig. 1e) show the typical diffraction peaks of SU-101, which are reasonably consistent with the simulated results.[31] Besides, the samples display strong diffraction peaks, indicating good crystallinity of the SU-101 NRs. More importantly, the crystalline structure of the SU-101 NRs could be well maintained over a wide pH region ranging from 2 to 14. The Fourier transform infrared (FT-IR) spectra indicated that there is coordination interaction between the metallic ions and hydroxyl group of ellagic acid, as shown by an obvious red shift in the C–OH stretching to 1363 nm from 1322 nm for the uncoordinated building blocks of ellagic acid (Fig. 1f).[32] It is worth mentioning that similar FT-IR spectra of the SU-101 NRs treated with different pH solutions could be observed, further indicating that the SU-101 NRs possess excellent chemical stability. X-ray photoelectron spectroscopy (XPS) characterization was also utilized to study the chemical composition and surface chemical state of the as-fabricated SU-101 NRs. The survey spectrum of the SU-101 NRs exhibited typical spectrum characteristics of Bi, C, O, and N elements (Fig. S4†). As exhibited in Fig. 1g, the binding energies of Bi 4f were located at 159.6 eV and 164.9 eV, which could be assigned to Bi $4f_{5/2}$ and Bi $4f_{7/2}$, respectively, suggesting that the oxidation state of Bi is +3. Thermogravimetric analysis (TGA) demonstrates that the SU-101 NRs show high thermal stability up to 300 °C (Fig. S5†). In addition, it was calculated that the Brunauer–Emmett–Teller surface area and average pore diameter of the SU-101 NRs are 25.96 $m^2\ g^{-1}$ and 20.43 nm, respectively (Fig. S6†).

The electrocatalytic CO_2RR performances of the SU-101 NRs were investigated in a typical three-electrode H-type cell. To confirm the reduction products, the liquid and the gas products were analyzed by nuclear magnetic resonance (NMR) spectroscopy (Fig. S7†) and online gas chromatography (GC) (Fig. S8†), respectively. The linear sweep voltammetry (LSV) curves of the SU-101 NRs in CO_2/N_2-saturated 0.5 M $KHCO_3$ aqueous solution

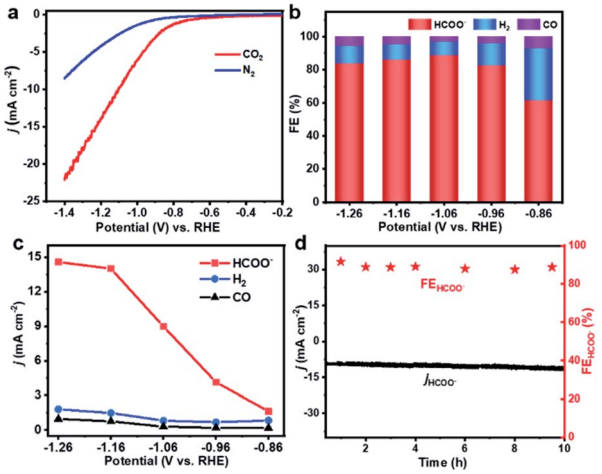

Fig. 2 Electrocatalytic CO_2RR performance of the SU-101 NRs. (a) LSV curves in N_2- (blue line) or CO_2- (red line) saturated 0.5 M $KHCO_3$ aqueous solution at a scan rate of 5 mV s^{-1}. (b) FEs of H_2, CO and $HCOO^-$ at different applied potentials. (c) Partial current densities of H_2, CO and $HCOO^-$. (d) Total current density and faradaic efficiency toward $HCOO^-$ over 10 h electrolysis at −1.06 V *vs.* RHE.

at a scan rate of 5 mV s^{-1} are presented in Fig. 2a. In N_2-saturated 0.5 M $KHCO_3$ electrolyte, the increase in the current below ~−0.70 V *vs.* RHE could be ascribed to the HER which is the main competing reaction during the CO_2RR. With the CO_2-purged 0.5 M $KHCO_3$ electrolyte, a dramatic increase of reductive current is observed at a potential of −0.56 V *vs.* RHE, which indicates the predominant occurrence of CO_2 reduction over the SU-101 catalyst.[33] Obviously, the SU-101 NRs displayed a higher cathode current density in CO_2-saturated solution than in N_2-saturated solution, manifesting their remarkable catalytic performances towards the CO_2RR. The conversion of CO_2 into $HCOO^-$ over the SU-101 catalyst occurred in the range from −0.86 to −1.26 V *vs.* RHE (Fig. 2b). Impressively, the highest FE of the SU-101 NRs could reach up to 93.66% at ~−1.06 V *vs.* RHE and a maximum formate partial current density (j_{HCOO^-}) of 14.57 mA cm^{-2} could be achieved at −1.26 V *vs.* RHE (Fig. 2c), which are comparable or even superior to those of recently reported Bi-based and other advanced catalysts (Fig. 3 and Table

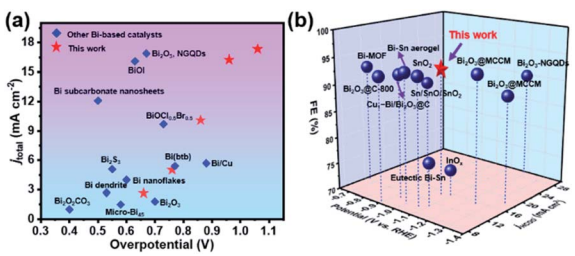

Fig. 3 (a) Literature overview of Bi-based electrocatalysts for the CO_2-to-formate conversion. Overpotentials (η) calculated using the equilibrium potential for $CO_2/HCOO^-$, E = −0.2 V *vs.* RHE.[34] (b) Comparison of partial current density and FE of formate for the SU-101 NRs with those of previously reported Bi-based and other advanced catalysts at the applied potentials.

S1†). Moreover, substantial quantities of $HCOO^-$ are produced with FE over 80.0% over a wide applied cathodic potential region ranging from ~−0.96 to ~−1.26 V *vs.* RHE. The long-term stability characterization of the SU-101 NRs was carried out at a constant potential of −1.06 V *vs.* RHE for 10 h. As presented in Fig. 2d, the FE of $HCOO^-$ could be maintained over 87.51% during 10 hours of continuous electrolysis and there was almost no evident deterioration in the current density and the NRs were well maintained after CO_2RR measurement (Fig. S9†), and the PXRD spectrum shows that the crystalline structure of the SU-101 NRs remains almost unchanged after the long-term stability test (Fig. S10†). The above-mentioned results demonstrate the superior structural robustness of the SU-101 NRs for the CO_2RR. In addition, the electrocatalytic CO_2RR performances of the SU-101 NRs in a flow cell were also investigated (Fig. S11–S13†). Note that the highest FE of the SU-101 NRs could reach up to 88.25% at ~−1.06 V *vs.* RHE and the partial current density towards formate is 40.46 mA cm^{-2} (Fig. S12†).

DFT calculations were performed to explore the possible molecular mechanisms for the CO_2RR and HER catalytic activities of SU-101 and gain insights into its high selectivity for formic acid production. As shown in Fig. 4, the crystal structure of SU-101 can be regarded as Bi_2O nanowires connected by ($C_{14}H_2O_8$) linkers in four directions, and its chemical composition is $Bi_2O(H_2O)_2(C_{14}H_2O_8)$. To save computational cost, we constructed a nanowire model, simplifying the two linkers on one side of the Bi_2O wire to ($C_2H_2O_2$), while leaving the two ($C_{14}H_2O_8$) linkers connected to the reaction site (Fig. 4b). The linker terminal oxygen is saturated with H and thus the chemical composition of the constructed nanowire is $Bi_2O(H_2O)_2(C_{14}H_2O_8)(C_2H_2O_2)$, which preserves the valence state of Bi^{3+} and its chemical environment. Three possible pathways were proposed for the CO_2RR (paths 1–3 in Fig. 4c). Path 1 leads to the production of CO, paths 2 and 3 lead to the yield of HCOOH and path 4 represents the HER pathway. The Bi^{3+} in the active sites is hexacoordinated and one of the ligands is the water molecule (Fig. 4b), and thus the active site is denoted as H_2O* (* represents the adsorption state). The energy profiles in Fig. 4b indicate that the first addition of H is the rate-determining step (RDS) and path 3 is the most favourable way leading to the generation of HCOOH since it has an energy barrier of only 0.87 eV for the RDS which is significantly lower than that of paths 1 and 2 (1.64 eV). The comparison of path 1 with path 2

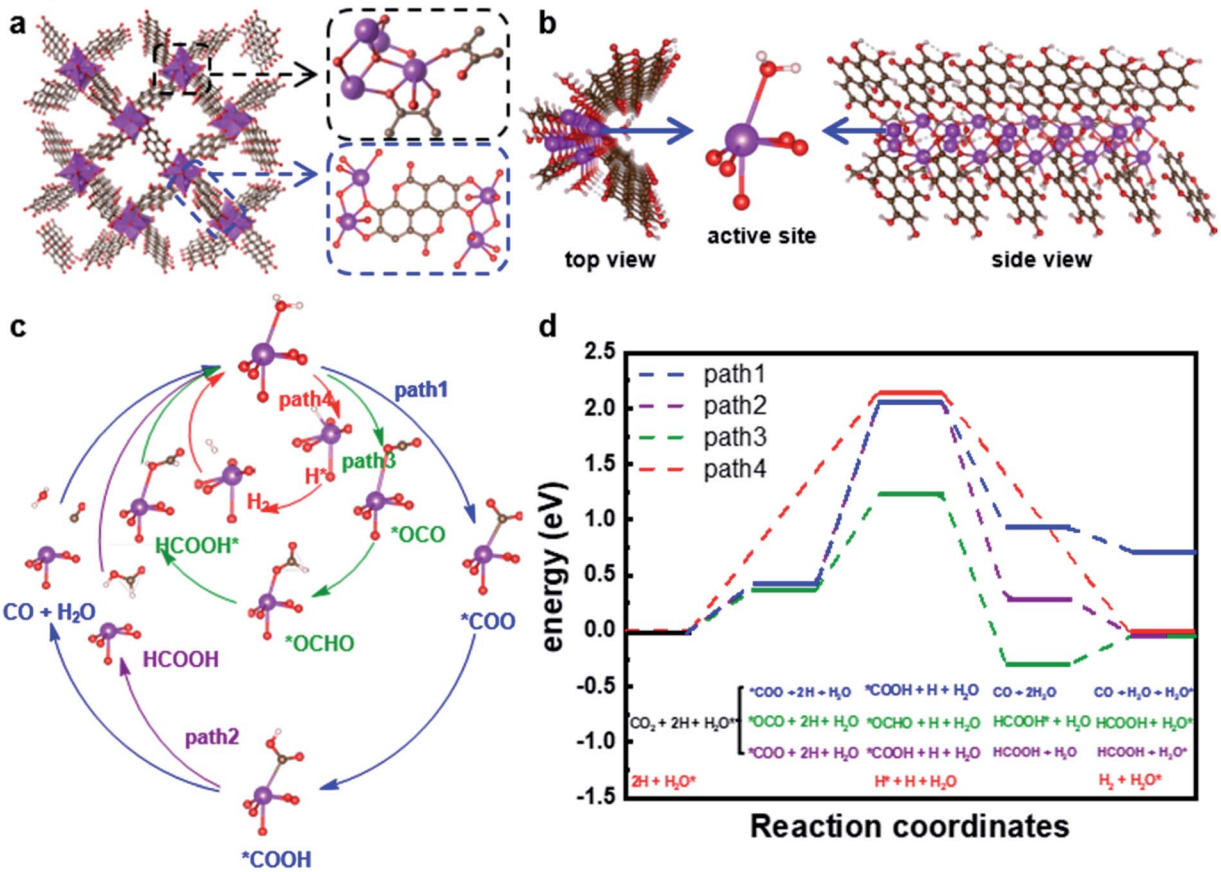

Fig. 4 (a) The crystal structure of the SU-101 and enlarged local structural details for the coordination microenvironment of Bi metal and the connection between Bi and the ($C_{14}H_2O_8$) linker. (b) The top and side views for the constructed nanowire periodic structure model mimicking SU-101 and the active site for the CO_2RR and HER. (c) Four proposed reaction pathways on the active site leading to different products which correspond to the CO_2RR and HER. (d) The energy profiles in eV for the four pathways proposed in (c) with material compositions provided.

also indicates the better selectivity for HCOOH production, which is rooted in that the adsorption of *COOH or ($*CO_2$) on the Bi^{3+} site is not strong enough to weaken the carbon–oxygen double bond, thus leading to the generation of hardly any CO. Path 4 responsible for the HER has the highest energy barrier of 2.13 eV, which indicates that the generation of H_2 is unfavourable. Thus, the easier adsorption of CO_2 than H makes the CO_2RR a more advantageous reaction than the HER, from which it is understandable that the O atom in CO_2 has stronger coordination capability than H. Moreover, as illustrated in Fig. S6,† the SU-101 catalyst exhibited a contact angle of 145.5° (Fig. S14†), demonstrating its inherent hydrophilic character which could contribute to inhibition of the competitive HER. The above results consistently indicate the high selectivity for HCOOH formation on SU-101, which corresponds well with the experimental results. This can be explained by two aspects: on one hand, the easier adsorption of CO_2 than H makes the CO_2RR a more advantageous reaction than the HER;[35,36] on the other hand, the adsorption of CO_2 on SU-101 is not strong enough to weaken the C=O bond and thus the CO generation is not favourable.

Conclusions

In summary, rod-shaped SU-101 catalysts were synthesized *via* a wet chemical method. Importantly, the crystalline structure of the SU-101 NRs could be well maintained over a wide pH region ranging from 2 to 14. The as-prepared SU-101 NRs exhibited high activity and selectivity toward $HCOO^-$ for electrochemical CO_2 reduction under ambient conditions. An exceptional FE of 93.66% for $HCOO^-$ production was achieved at a potential of −1.06 V *vs.* RHE with an outstanding stability over 10 h. Theoretical calculations confirm that the suitable adsorption strength of SU-101 to CO_2 is the reason for its high selectivity for $HCOO^-$ production: neither so weak as to allow the HER to occur preferentially, nor so strong as to cause CO formation. This work offers new opportunities for developing and designing highly stable framework structures for the electrochemical conversion of CO_2 into value-added products.

Author contributions

Junjun Li, Congyong Wang, Dingjia Wang and Chenhuai Yang contributed equally to this work.

Conflicts of interest

There are no conflicts to declare.

Acknowledgements

This work was supported by the National Natural Science Foundation of China (22071172, 91833306, 21875158, 51633006, and 51733004). We thank the Haihe Laboratory of Sustainable Chemical Transformations for financial support.

References

1 K. Sordakis, C. Tang, L. K. Vogt, H. Junge, P. J. Dyson, M. Beller and G. Laurenczy, *Chem. Rev.*, 2018, **118**, 372–433.
2 D. H. Nam, P. De Luna, A. Rosas-Hernandez, A. Thevenon, F. Li, T. Agapie, J. C. Peters, O. Shekhah, M. Eddaoudi and E. H. Sargent, *Nat. Mater.*, 2020, **19**, 266–276.
3 P. Deng, F. Yang, Z. Wang, S. Chen, Y. Zhou, S. Zaman and B. Y. Xia, *Angew. Chem., Int. Ed.*, 2020, **59**, 10807–10813.
4 N. Wang, K. Yao, A. Vomiero, Y. Wang and H. Liang, *SmartMat*, 2021, **2**, 423–425.
5 Y. Wang, X. Zheng and D. Wang, *Nano Res.*, 2022, **15**, 1730–1752.
6 S. Chen, W.-H. Li, W. Jiang, J. Yang, J. Zhu, L. Wang, H. Ou, Z. Zhuang, M. Chen, X. Sun, D. Wang and Y. Li, *Angew. Chem., Int. Ed.*, 2022, **61**, e202114450.
7 J. Li, S. U. Abbas, H. Wang, Z. Zhang and W. Hu, *Nano-Micro Lett.*, 2021, **13**, 216.
8 Z. Gao, J. Li, Z. Zhang and W. Hu, *Chin. Chem. Lett.*, 2022, **33**, 2270–2280.
9 Y. Zhu, X. Cui, H. Liu, Z. Guo, Y. Dang, Z. Fan, Z. Zhang and W. Hu, *Nano Res.*, 2021, **14**, 4471–4486.
10 Z. Gao, C. Wang, J. Li, Y. Zhu, Z. Zhang and W. Hu, *Acta Phys.-Chim. Sin.*, 2021, **37**, 2010025.
11 P. Lamagni, M. Miola, J. Catalano, M. S. Hvid, M. A. H. Mamakhel, M. Christensen, M. R. Madsen, H. S. Jeppesen, X. M. Hu, K. Daasbjerg, T. Skrydstrup and N. Lock, *Adv. Funct. Mater.*, 2020, **30**, 1910408.
12 J. Yang, X. Wang, Y. Qu, X. Wang, H. Huo, Q. Fan, J. Wang, L. M. Yang and Y. Wu, *Adv. Energy Mater.*, 2020, **10**, 2001709.
13 M. Zhang, W. Wei, S. Zhou, D.-D. Ma, A. Cao, X.-T. Wu and Q.-L. Zhu, *Energy Environ. Sci.*, 2021, **14**, 4998–5008.
14 Z. H. Zhu, B. H. Zhao, S. L. Hou, X. L. Jiang, Z. L. Liang, B. Zhang and B. Zhao, *Angew. Chem., Int. Ed.*, 2021, **60**, 23394–23402.
15 Z. Wu, H. Wu, W. Cai, Z. Wen, B. Jia, L. Wang, W. Jin and T. Ma, *Angew. Chem., Int. Ed.*, 2021, **60**, 12554–12559.
16 J. Li, Z. Zhang and W. Hu, *Green Energy Environ.*, 2022, DOI: **10.1016/j.gee.2021.11.004**.
17 T. Zheng, C. Liu, C. Guo, M. Zhang, X. Li, Q. Jiang, W. Xue, H. Li, A. Li, C. W. Pao, J. Xiao, C. Xia and J. Zeng, *Nat. Nanotechnol.*, 2021, **16**, 1386–1393.
18 H. Yang, N. Han, J. Deng, J. Wu, Y. Wang, Y. Hu, P. Ding, Y. Li, Y. Li and J. Lu, *Adv. Energy Mater.*, 2018, **8**, 1801536.
19 N. Han, P. Ding, L. He, Y. Li and Y. Li, *Adv. Energy Mater.*, 2019, **10**, 1902338.
20 E. Zhang, T. Wang, K. Yu, J. Liu, W. Chen, A. Li, H. Rong, R. Lin, S. Ji, X. Zheng, Y. Wang, L. Zheng, C. Chen, D. Wang, J. Zhang and Y. Li, *J. Am. Chem. Soc.*, 2019, **141**, 16569–16573.
21 K. Ye, Z. Zhou, J. Shao, L. Lin, D. Gao, N. Ta, R. Si, G. Wang and X. Bao, *Angew. Chem., Int. Ed.*, 2020, **59**, 4814–4821.
22 H. Wu, M. Zeng, X. Zhu, C. Tian, B. Mei, Y. Song, X.-L. Du, Z. Jiang, L. He, C. Xia and S. Dai, *ChemElectroChem*, 2018, **5**, 2717–2721.

23 M. K. Birhanu, M.-C. Tsai, A. W. Kahsay, C.-T. Chen, T. S. Zeleke, K. B. Ibrahim, C.-J. Huang, W.-N. Su and B.-J. Hwang, *Adv. Mater. Interfaces*, 2018, **5**, 1800919.
24 Y. Wang, P. Hou, Z. Wang and P. Kang, *ChemPhysChem*, 2017, **18**, 3142–3147.
25 N. Devarajan and P. Suresh, *Org. Chem. Front.*, 2018, **5**, 2322–2331.
26 W. Guo, X. Sun, C. Chen, D. Yang, L. Lu, Y. Yang and B. Han, *Green Chem.*, 2019, **21**, 503–508.
27 Q. Mu, W. Zhu, G. Yan, Y. Lian, Y. Yao, Q. Li, Y. Tian, P. Zhang, Z. Deng and Y. Peng, *J. Mater. Chem. A*, 2018, **6**, 21110–21119.
28 F. Li, G. H. Gu, C. Choi, P. Kolla, S. Hong, T.-S. Wu, Y.-L. Soo, J. Masa, S. Mukerjee, Y. Jung, J. Qiu and Z. Sun, *Appl. Catal., B*, 2020, **277**, 119241.
29 K. Ye, A. Cao, J. Shao, G. Wang, R. Si, N. Ta, J. Xiao and G. Wang, *Sci. Bull.*, 2020, **65**, 711–719.
30 C. Cao, D. D. Ma, J. F. Gu, X. Xie, G. Zeng, X. Li, S. G. Han, Q. L. Zhu, X. T. Wu and Q. Xu, *Angew. Chem., Int. Ed.*, 2020, **59**, 15014–15020.
31 E. S. Grape, J. G. Flores, T. Hidalgo, E. Martinez-Ahumada, A. Gutierrez-Alejandre, A. Hautier, D. R. Williams, M. O'Keeffe, L. Ohrstrom, T. Willhammar, P. Horcajada, I. A. Ibarra and A. K. Inge, *J. Am. Chem. Soc.*, 2020, **142**, 16795–16804.
32 H. Wang, X. Xu, C. Lee, C. Johnson, K. Sohlberg and H.-F. Ji, *J. Phys. Chem. C*, 2012, **116**, 4442–4448.
33 Q. Li, J. Fu, W. Zhu, Z. Chen, B. Shen, L. Wu, Z. Xi, T. Wang, G. Lu, J. J. Zhu and S. Sun, *J. Am. Chem. Soc.*, 2017, **139**, 4290–4293.
34 C. W. Li and M. W. Kanan, *J. Am. Chem. Soc.*, 2012, **134**, 7231–7234.
35 L. Liu, K. Yao, J. Fu, Y. Huang, N. Li and H. Liang, *Colloids Surf., A*, 2022, **633**, 127840.
36 Y. Xue, C. Li, X. Zhou, Z. Kuang, W. Zhao, Q. Zhang and H. Chen, *ChemElectroChem*, 2022, **9**, e202101648.